SCIENCE CHINA PRESS

SCIENCE CHINA Life Sciences
life.scichina.com link.springer.com
https://doi.org/10.1007/s11427-024-2707-9

RESEARCH PAPER

Optimizing ABA-based chemically induced proximity for enhanced intracellular transcriptional activation and modification response to ABA

Zeng Zhou[1,3†], Yue-Qi Wang[2†], Xu-Nan Zheng[2], Xiao-Hong Zhang[3], Lu-Yao Ji[3], Jun-You Han[2], Ze-Cheng Zuo[2*], Wei-Liang Mo[2*] & Li Zhang[2*]

[1]College of Life Sciences, Fujian Agriculture and Forestry University, Fuzhou 350002, China;
[2]Jilin Province Engineering Laboratory of Plant Genetic Improvement, College of Plant Science, Jilin University, Changchun 130062, China;
[3]Basic Forestry and Proteomics Research Center, Fujian Agriculture and Forestry University, Fuzhou 350002, China

†Contributed equally to this work
*Corresponding authors (Ze-Cheng Zuo, email: zuozhecheng@jlu.edu.cn; Wei-Liang Mo, email: mowl@jlu.edu.cn; Li Zhang , email: zhang_li18@mails.jlu.edu.cn)

Received 3 July 2024; Accepted 7 August 2024; Published online 19 August 2024

Abscisic acid (ABA)-based chemically induced proximity (CIP) is primarily mediated by the interaction of the ABA receptor pyrabactin resistance 1-like 1 (PYL1) and the 2C-type protein phosphatase ABI1, which confers ABA-induced proximity to their fusion proteins, and offers precise temporal control of a wide array of biological processes. However, broad application of ABA-based CIP has been limited by ABA response intensity. In this study, we demonstrated that ABA-induced interaction between another ABA receptor pyrabactin resistance 1 (PYR1) and ABI1 exhibited higher ABA response intensity than that between PYL1 and ABI1 in HEK293T cells. We engineered PYR1-ABI1 and PYL1-ABI1 into ABA-induced transcriptional activation tools in mammalian cells by integration with CRISPR/dCas9 and found that the tool based on PYR1-ABI1 demonstrated better ABA response intensity than that based on PYL1-ABI1 for both exogenous and endogenous genes in mammalian cells. We further achieved ABA-induced RNA m^{6}A modification installation and erasure by combining ABA-induced PYR1-ABI1 interaction with CRISPR/dCas13, successfully inhibiting tumor cell proliferation. We subsequently improved the interaction of PYR1-ABI1 through phage-assisted continuous evolution (PACE), successfully generating a PYR1 mutant (PYR1m) whose interaction with ABI1 exhibited a higher ABA response intensity than that of the wild-type. In addition, we tested the transcriptional activation tool based on PYRm-ABI1 and found that it also showed a higher ABA response intensity than that of the wild type. These results demonstrate that we have developed a novel ABA-based CIP and further improved upon it using PACE, providing a new approach for the modification of other CIP systems.

ABA | chemically induced proximity | transcriptional activation | m^{6}A modification | protein evolution

INTRODUCTION

Biological processes are often regulated by the spatial proximity of different biomolecules within cells (Stanton et al., 2018). The proximity of proteins, or protein-protein interaction, plays a vital role in cell signaling and the maintenance of cellular integrity (Ziegler et al., 2021). In recent years, significant advances have been made in the development of tools for studying and manipulating protein proximity. Among these tools, chemically induced proximity (CIP) has garnered widespread attention. CIP is a technology based on the chemical induction of specific receptor-ligand interactions, resulting in the induction of protein proximity. CIP offers such advantages as low toxicity, rapid and reversible dynamics suitable for dynamic studies, fast dose responses, high efficiency, and temporal control (Ziegler et al., 2021; Bottone et al., 2023). This technique has successfully and precisely controlled various biological processes, including signal transduction (Feng et al., 2014), transcriptional regulation (Zetsche et al., 2015), RNA base editing (Yu et al., 2024), protein degradation (Daniel et al., 2018), phase separation (Hernandez-Candia et al., 2024) and apoptosis (Gourisankar et al., 2023).

Research has indicated that the genesis of most tumors is predominantly directed by driver genes (Stratton et al., 2009; Stratton, 2011). By inhibiting the function of driver genes, the corresponding tumors will cease to grow. Over the past few decades, targeted therapy has seen rapid development. Targeted therapy is a cancer treatment method that uses small molecule drugs or monoclonal antibodies to target driver genes or proteins and inhibit their functions, thereby interfering with the growth, division, and spread of tumor cells (Min and Lee, 2022). Common targets include oncoproteins such as human epidermal growth factor receptor 2 (HER2), epidermal growth factor receptor (EGFR), and MYC (Ke and Shen, 2017). Additionally, an increasing body of research suggests that RNA modifications such as m^{6}A are closely linked to the occurrence, progression, and prognosis of tumors (Deng et al., 2022). This is because m^{6}A affects the expression of both tumor suppressor genes and oncogenes. Through the CIP system, we can manipulate gene transcription, m^{6}A modification, or protein degradation within tumor cells to inhibit tumor development. As a result, CIP is emerging as a novel strategy

for targeted therapies.

CIP based on plant hormones such as abscisic acid (ABA), gibberellin (GA), and indole acetic acid (IAA) have emerged as powerful tools in the regulation of cellular processes in mammalian cells due to their flexibility and heterogeneity (Gao et al., 2016; Bao et al., 2017; Chen et al., 2017; Daniel et al., 2018; Li et al., 2019; Ziegler et al., 2021; Shi et al., 2022). Due to its oral availability, non-toxicity, and low cost (Liang et al., 2011), the ABA-based CIP, which primarily involves the ABA receptor pyrabactin resistance 1-like 1 (PYL1) and the 2C-type protein phosphatase (PP2C) ABI1, has been extensively studied (Gao et al., 2016; Chen et al., 2017; Shi et al., 2022). However, there exist other plant ABA receptors, including pyrabactin resistance 1 (PYR1) and PYL2-14, that have similar or strong interactions (Cutler et al., 2010).For example, the interaction between PYR1 and ABI1 has been shown to be stronger than that between PYL1 and ABI1 (Nemoto et al., 2018). Despite this, few studies have explored the development of ABA-based CIP systems using the ABA receptor PYR1, and there is a lack of research using the PYR1-ABI1 mediated CIP in mammalian cells. Moreover, though the response intensity induced by CIP is crucial for precise temporal control. However, there is a notable absence of research on modifying ABA receptors to enhance the response intensity of ABA-based CIP systems for their practical use in regulating cellular processes.

While the directed evolution of proteins can enhance their functional performance, the process requires a relatively long duration and intricate equipment (Xie et al., 2022). Phage-assisted continuous evolution (PACE), a simple and efficient protein-directed evolution system developed by David R. Liu and coworkers (Esvelt et al., 2011), has been successfully applied in the evolution of proteins such as Cas9 (Hu et al., 2018; Miller et al., 2020b), proteinases (Packer et al., 2017; Blum et al., 2021), single-base editors (Thuronyi et al., 2019; Richter et al., 2020), and prime editors (Doman et al., 2023). In the field of biomolecular interactions, PACE has been used to enhance the affinity of protein-DNA (Esvelt et al., 2011) and protein-protein interactions (Badran et al., 2016; Ye et al., 2020). While it is evident that protein evolution finds diverse applications, PACE has not been applied in the evolution of small molecule-induced protein-protein interactions.

In this study, we established a novel transcriptional activation tool based on ABA-induced PYR1-ABI1 interaction in mammalian cells. We determined that ABA-induced PYR1-ABI1 interaction exhibits higher response intensity than that of PYL1-ABI1. Our findings indicate that this tool possesses higher ABA response intensity than that based on PYL1-ABI1. We subsequently combined ABA-induced PYR1-ABI1 interaction with CRISPR/dCas13 technology to achieve ABA-induced installation and removal of RNA m^{6}A modifications. Upon ABA induction, we reduced the m^{6}A level of *MYC* mRNA, suppressing the proliferation of tumor cells. Finally, we established the PACE system for evolving ABA-induced PYR1-ABI1 interaction. After 252 h of evolution, we obtained a PYR1 mutant that showed an enhanced ABA response intensity compared with the wild type. In summary, this study provides highly responsive ABA-based CIP tools for regulating transcriptional and m^{6}A modifications. These tools are not only valuable for studying specific gene transcriptional regulation and m^{6}A modifications but also hold significant potential in the development of targeted therapeutic tools.

RESULTS

A novel ABA-induced transcriptional activation system in mammalian cells

Previous research has demonstrated that the interaction between PYR1 and ABI1 is significantly enhanced by the addition of 100 μmol L^{-1} ABA in *Arabidopsis thaliana* (Nishimura et al., 2010). To assess whether this interaction occurs in HEK293T cells, we performed a biomolecular fluorescence complementation (BiFC) assay. While we observed a faint reconstituted YFP fluorescence signal in the absence of ABA, the interaction between PYR1 and ABI1 led to a pronounced increase in the reconstituted YFP fluorescence signal in the presence of 100 μmol L^{-1} ABA (Figure 1A), indicating that ABA significantly enhances the interaction between PYR1 and ABI1 in HEK293T cells. We further investigated the interaction between PYR1 and ABI1 using Split Luciferase assay and co-immunoprecipitation (co-IP) assay. The reconstituted bioluminescence resulting from the interaction between PYR1 and ABI1 significantly increased in response to 100 μmol L^{-1} ABA (Figure 1B). Moreover, the Co-IP signal of PYR1 showed a substantial enhancement (Figure 1C). These results suggest that PYR1 interacts with ABI1 in an ABA-enhanced manner in HEK293T cells.

Before establishing the ABA-induced transcription activation system, we first assessed the toxicity of ABA in various cell types and observed that ABA exhibited no toxicity toward any tested cell types (Figure S1 in Supporting Information). We then validated the efficiency of single guide RNAs (sgRNAs) using a dCas9-VPR mediated reporter gene activation assay. Different sgRNAs were designed for the reporter genes *Luc* and *Ren*, which are driven by *FT G* and SV40 promoter, respectively (Figure S2A and B in Supporting Information). The *FT G* segment, an intron of the flowering gene *FLOWERING LOCUS T* (*FT*) in *Arabidopsis thaliana*, can be bound by its transcriptional activators in HEK293T cells to initiate transcription of downstream reporter genes (Liu et al., 2008; Yang et al., 2018). As shown in Figure S2C and D, the expression of Luc and Ren in cells co-expressing reporter genes, dCas9-VPR, and sgRNA increased by 24.6-fold and 20.9-fold, respectively, compared with cells transfected with the reporter only. These findings indicate that sgRNAs exhibit a notably high efficiency in HEK293T cells.

To flexibly control gene expression, we developed an ABA-induced transcriptional activation system that integrates ABA-induced PYR1-ABI1 interaction with the split-dCas9 method (Figure S2E in Supporting Information). We first tested the effects of exchanging dimerization domains between the dCas9$^{N1–535}$ and dCas9$^{C536–1368}$-VPR and found that PYR1-dCas9$^{N1–535}$ and ABI1-dCas9$^{C536–1368}$-VPR, which we named ABA Split-dCas9-VPR, exhibited an effective ABA response (Figure S2F in Supporting Information).

Despite the ABA responsiveness of the ABA Split-dCas9-VPR system, its efficiency in activating the transcription of target genes was not remarkable. To develop a more efficient ABA-induced transcriptional activation system, we fused PYR1 with VPR and ABI1 with dCas9, allowing for the ABA-induced assembly of dCas9 and VPR, referred to as ABA dCas9-VPR.

To compare the transcription activation efficiency between ABA dCas9-VPR and ABA Split-dCas9-VPR, we conducted Luc or Ren luciferase reporter gene activation assays (Figure 1D and F) in HEK293T cells. As shown in Figure 1E and G, the activation

https://doi.org/10.1007/s11427-024-2707-9

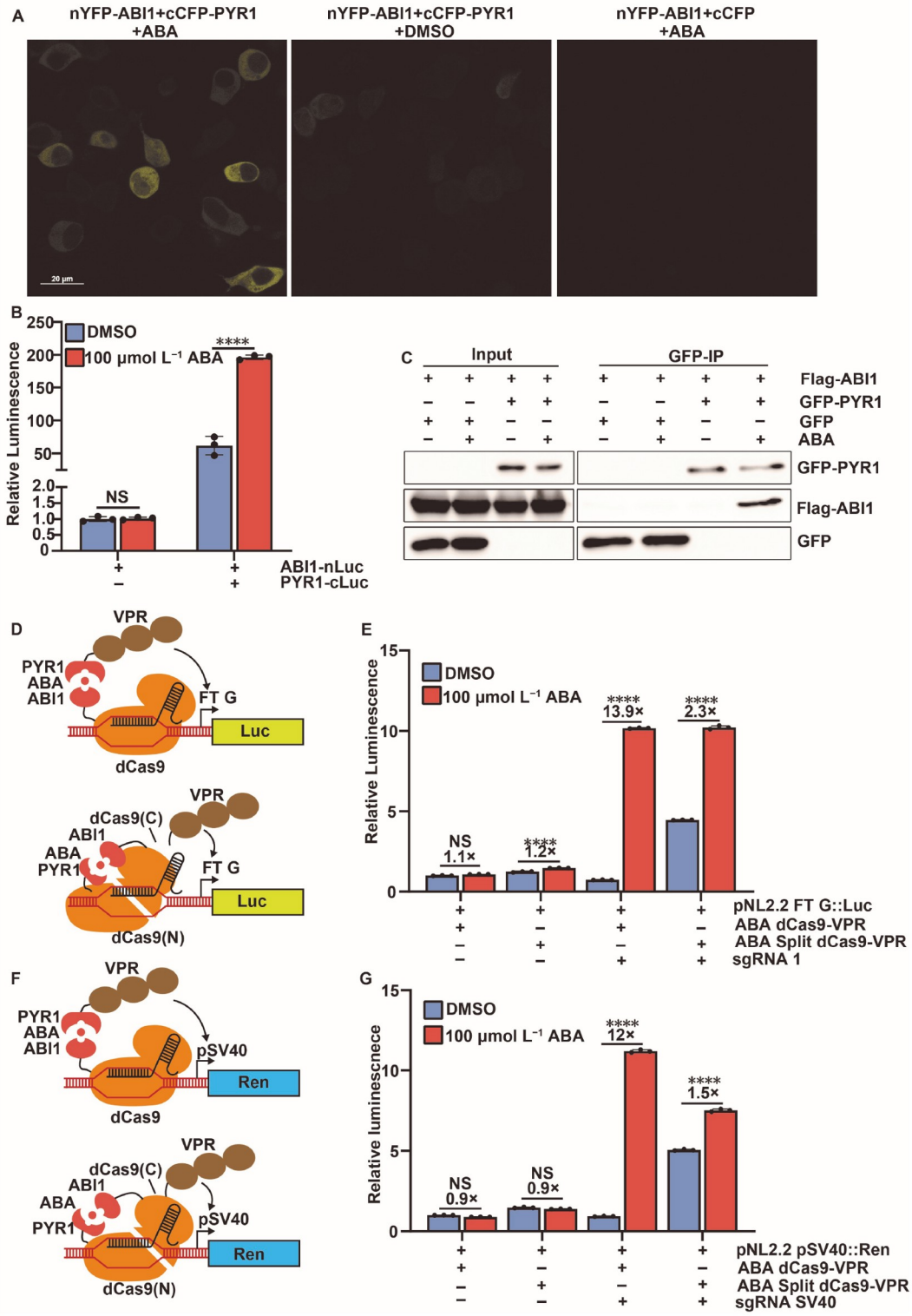

Figure 1. A novel ABA-induced transcriptional activation system in mammalian cells. A, BiFc assays showing ABA-enhanced interaction between PYR1 and ABI1 in HEK293T cells. Cells co-transfected with plasmids expressing the respective proteins were treated with or without 100 μmol L^{-1} ABA treatment for 24 h. Scale bar, 20 μm. B, Split Luciferase assay showing ABA-enhanced interaction between PYR1 and ABI1 in HEK293T cells. Cells co-transfected with plasmids expressing ABI1-nLuc and cLuc were as the negative control. Data were normalized to the bioluminescence of negative control and presented as mean±SD (n=3). NS, no significance; ****, P<0.0001 (Two-tailed student's t-test). C, Co-immunoprecipitation (Co-IP) assay showing ABA-enhanced interaction between PYR1 and ABI1 in HEK293T cells. Transfected cells were treated with DMSO or 100 μmol L^{-1} ABA for 24 h. The IP signals were detected using anti-GFP or anti-Flag. (D, F) Schematic of two kind of ABA-induced transcriptional activation system (upper, ABA dCas9-VPR system, under, ABA Split-dCas9-VPR system) for *Luc* (D) or *Ren* (F) activation. E and G, Bioluminescence analysis of two kind of ABA-induced transcriptional activation system for *Luc* (E) or *Ren* (G) activation in HEK293T cells. Transfected cells were treated with DMSO or 100 μmol L^{-1} ABA for 24 h. Data are normalized to the bioluminescence of cells transfected with pUC19 vector (no-sgRNA control) under the treatment of DMSO and presented as mean±SD (n=3). NS, no significance; ****, P<0.0001 (two way ANOVA followed by Bonferroni's multiple comparisons test).

levels of Luc and Ren induced by ABA dCas9-VPR were much higher than those of ABA Split-dCas9-VPR under ABA treatment. When compared with cells without transfected sgRNA, ABA dCas9-VPR resulted in a decrease of 30% and 10% in Luc and Ren expression levels, respectively, while ABA Split-dCas9-VPR increased the expression of Luc by 3.6-fold and Ren by 3.4-fold in the absence of ABA treatment. These data suggest that the spatial hindrance effect of the dCas9 protein may affect transcription (Qi et al., 2013) and split dCas9 proteins may possess intrinsic complementation capability (Zetsche et al., 2015). These results indicate that ABA dCas9-VPR exhibits stronger ABA-induced transcriptional activation efficiency and lower leakage activation levels in the absence of ABA.

Furthermore, it is worth noting that ABA dCas9-VPR system also possesses the advantage of reversibility. As shown in Figure S3, PYR1-VPR significantly activated the expression of Ren after 12 h of ABA treatment. Removal of ABA after 12 h decreased Ren levels markedly, indicating the reversibility of ABA dCas9-VPR system. The result supports the flexible transcriptional regulation of ABA dCas9-VPR system.

Comparison of transcriptional activation tools based on PYR1-ABI1 and PYL1-ABI1

It has been reported that the interaction of PYR1-ABI1 induced by ABA is stronger than that of PYL1-ABI1 (Nemoto et al., 2018). To compare the differences in interaction between PYR1-ABI1 and PYL1-ABI1 in HEK293T cells, the kinetics of their interactions were determined using Split Luciferase assay. As shown in Figure S4A and B, both the PYR1-ABI1 and PYL1-ABI1 interactions gradually strengthened with increasing ABA concentrations, reaching their peaks at a concentration of 100 μmol L^{-1} ABA. However, when comparing the peak values of bioluminescence, we found that the PYL1-ABI1 interaction was stronger than the PYR1-ABI1 interaction (Figure 2A), which is contrary to the previous report. Intriguingly, further analysis of the ABA response intensity (Luc^{+ABA}/Luc^{-ABA}) of the PYR1-ABI1 and PYL1-ABI1 interactions revealed that the ABA response intensity of the PYR1-ABI1 interaction induced by ABA was higher than that of PYL1-ABI1 (Figure 2B; Figure S4C and D in Supporting Information). We therefore hypothesized that the transcriptional activation tool based on PYR1-ABI1 might have a higher ABA response.

To validate this hypothesis, we compared the activation ability of the tools based on PYR1-ABI1 or PYL1-ABI1. We found that the *Ren* activation level (the ratio of bioluminescence under ABA treatment to that under DMSO treatment) induced by PYR1-VPR was consistently higher than that of PYL1-VPR under different concentrations of ABA with similar expression levels of PYR1-VPR and PYL1-VPR (Figure 2C; Figure S5 in Supporting Information). Furthermore, we detected the bioluminescence at different time points after ABA treatment and found that the *Ren* activation level induced by PYR1-VPR was much higher than that of PYL1-VPR at 12, 18, and 24 h post-treatment (Figure 2D). These findings confirm that the transcriptional activation tool based on PYR1-ABI1 has a higher ABA response.

ABA-induced transcriptional activation of endogenous genes

After evaluating the capability of transcriptional activation tools based on PYR1-ABI1 or PYL1-ABI1 using reporter gene activation assays, we proceeded to validate the ability of these two tools to activate endogenous genes. For this purpose, we selected many genes associated with cellular development and tumor suppression. Since multiple gRNAs targeting the same gene can result in higher levels of gene transcription activation (Chavez et al., 2016), we designed four gRNAs that bind to the promoter region of each gene (Figure S6A and 3A in Supporting Information). One of the chosen genes, titin (TTN), plays a critical role in the assembly and function of striated muscles in vertebrates (Mayans et al., 1998). Previous studies have demonstrated efficient transcriptional activation of *TTN* by the dCas9-VPR fusion protein (Chavez et al., 2015; Chavez et al., 2016). Here we found that the transcriptional activation tool based on PYR1-ABI1 could activate *TTN* transcription up to 9335-fold under ABA induction in HEK293T cells (Figure S6B in Supporting Information).

G protein-coupled estrogen receptor 1 (GPER1) and P53 function as tumor suppressors and are downregulated in various tumor cells (Liang et al., 2021; Cao et al., 2022). Our findings indicate that *GPER1* was significantly activated by the transcriptional activation tool based on PYR1-ABI1 both in SUM159PT and HEK293T cells under ABA induction (Figure 3B; Figure S6C in Supporting Information). Interestingly, the level of *GPER1* transcriptional activation was markedly higher in HEK293T cells than in SUM159PT cells which may be attributed to differential basal expression levels of GPER1 in different cell types (Chavez et al., 2015).

We subsequently assessed the ABA response intensity of transcriptional activation tools based on PYR1-ABI1 and PYL1-ABI1 in activating tumor suppressors (*GPER1* and *TP53*). The ABA response intensity of transcriptional activation refers to the ratio of transcription levels under ABA treatment to those under DMSO treatment. As shown in Figure 3C and D, upon ABA induction, PYR1-VPR increased *GPER1* and *TP53* expression by 46.6- and 4.4-fold, respectively, both of which were higher than those of PYL1-VPR (40.8- and 2.9-fold, respectively). To determine whether transcriptional activation tools based on PYR1-ABI1 exhibits higher ABA response intensity than that based on PYL1-ABI1 in activating other genes, we compared the efficiency of PYR1-ABI1 and PYL1-ABI1 in activating other genes, including *HBG1*, *MIAT* and *CXCR4*, which were activated efficiently by the dCas9-VPR system (Chavez et al., 2016). qRT-PCR results revealed that under ABA induction, PYR1-VPR led to higher fold changes of *HBG1*, *MIAT* and *CXCR4* expression than PYL1-VPR in 293T cells (Figure S7 in Supporting Information). These are consistent with the results of our previous reporter gene activation experiments, indicating that the transcriptional activation tool based on PYR1-ABI1 exhibits a higher ABA response for endogenous genes activation.

ABA-induced RNA m^6A installation and removal

The CRISPR-associated nuclease Cas13, when guided by gRNA, can bind and cleave ssRNA (Cox et al., 2017). Although nuclease-deactivated Cas13 (dCas13) lacks cleavage activity, it retains the ability to bind ssRNA when guided by gRNA, making it a sequence-specific RNA-binding domain (Cox et al., 2017). N^6-methyladenosine (m^6A) is the most common modification of eukaryotic mRNA, involved in the regulation of RNA splicing (Zhao et al., 2014), nuclear export (Roundtree et al., 2017), RNA

https://doi.org/10.1007/s11427-024-2707-9

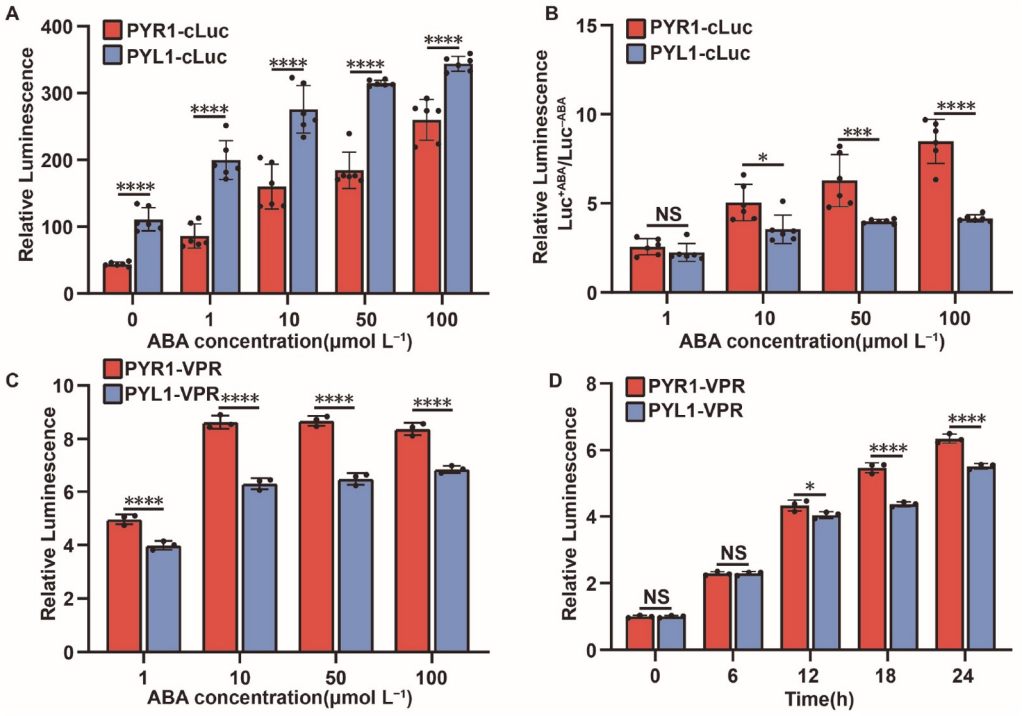

Figure 2. Comparison of transcriptional activation tools based on PYR1-ABI1 and PYL1-ABI1. A, Bioluminescence analysis of HEK293T cells co-transfected with the plasmids expressing ABI1-nLuc and PYR1-cLuc or PYL1-cLuc, respectively. Transfected cells were treated with DMSO (0 μmol L^{-1}) or ABA (1, 10, 50, 100 μmol L^{-1}) for 24 h prior to bioluminescence measurement. The bioluminescence was collected every two minutes. Data are normalized to the bioluminescence of cells expressing ABI1-nLuc and cLuc under the treatment of 100 μmol L^{-1} ABA at the first timepoint. The peaks of bioluminescence are shown. Data are presented as mean±SD (n=6). ****, P<0.0001 (two-way ANOVA followed by Bonferroni's multiple comparisons test). B, Bioluminescence analysis of HEK293T cells co-transfected with the plasmids expressing ABI1-nLuc and PYR1-cLuc or PYL1-cLuc under ABA treatment (1, 10, 50, 100 μmol L^{-1}), respectively. The bioluminescence at the first time point are shown. Data are normalized to the bioluminescence of cells treated with DMSO and presented as mean±SD (n=6). NS, no significance; *, P<0.05; ***, P<0.001; ****, P<0.0001 (two-way ANOVA followed by Bonferroni's multiple comparisons test). C, HEK293T cells expressing pSV40-Ren, ABI1-dCas9, and sgRNA SV40 were co-transfected with the plasmids expressing PYR1-VPR or PYL1-VPR, respectively. Transfected cells were treated with DMSO (0 μmol L^{-1}) or ABA (1, 10, 50, 100 μmol L^{-1}) for 24 h prior to bioluminescence measurement. Data are normalized to the bioluminescence of cells treated with DMSO and presented as mean±SD (n=3). NS, no significance; ****, P<0.0001 (two-way ANOVA followed by Bonferroni's multiple comparisons test). D, HEK293T cells expressing pSV40-Ren, ABI1-dCas9, and sgRNA SV40 were co-transfected with the plasmids expressing PYR1-VPR or PYL1-VPR, respectively. Transfected cells were treated with 100 μmol L^{-1} ABA for 0, 6, 12, 18, 24 h prior to bioluminescence measurement. Data are normalized to the bioluminescence of cells treated with DMSO and presented as mean±SD (n=3). NS, no significance; *, P<0.05; ****, P<0.0001 (two-way ANOVA followed by Bonferroni's multiple comparisons test).

stability (Wang et al., 2014), and translation efficiency (Wang et al., 2015). The installation of mRNA m^6A modification is mediated by the core methyltransferase complex ("writers"), including methyltransferase-like 3 (Mettl3)/methyltransferase-like 14 (Mettl14)/Wilms' tumor 1-associated protein (WATP), while its removal is carried out by the demethylases ("erasers"), including fat-mass and obesity-associated protein (FTO) and AlkB homolog 5 (ALKBH5) (Deng et al., 2022). Previous studies have fused dCas13 with Mettl3, FTO, or ALKBH5 to achieve targeted installation or removal of m^6A modifications (Li et al., 2020; Wilson et al., 2020; Wei et al., 2022).

To further expand upon the application of the CIP system based on PYR1-ABI1 in regulating cellular processes, we developed ABA-induced RNA m^6A modification regulatory tools using CRISPR/dCas13 technology (Figure 3E). We constructed an ABA-induced RNA m^6A installation tool named ABA dCas13b-M3 by fusing PYR1 with M3 (Mettl3 lacking the zinc finger RNA-binding domain), and ABI1 with dCas13b from *Prevotella* sp. P5–125 (referred to as dCas13b hereafter). We also fused PYR1 with either the catalytic domain of FTO (FALK) or the catalytic domain of ALKBH5 (ALK) and ABI1 with dCas13b to obtain the ABA-induced RNA m^6A removal tools ABA dCas13b-FALK and ABA dCas13-ALK. We then selected the A690 site in the coding region of *GAPDH* mRNA as a target for m^6A installation with ABA dCas13b-M3, for which had low methylation reported in previous research (Wilson et al., 2020). As shown in Figure 3F, ABA dCas13b-M3 slightly increased the m^6A level of *GAPDH* mRNA under ABA induction.Studies have shown that the mRNA of the oncogene *MYC* undergoes m^6A modification and positively regulates tumor cell proliferation (Meyer et al., 2012; Li et al., 2020). To determine whether ABA dCas13b-FALK and ABA dCas13b-ALK can induce targeted erasure of m^6A modification in tumor cells, we targeted *MYC* mRNA. We found that ABA dCas13b-FALK slightly decreased the m^6A level of *MYC* mRNA under ABA induction (Figure 3G), while ABA dCas13b-ALK significantly reduced the m^6A level of *MYC* mRNA under ABA induction (Figure 3H). Further cell proliferation experiments demonstrated that ABA dCas13b-ALK, together with gRNA targeting *MYC* mRNA, could inhibit the proliferation of HeLa cells under ABA induction (Figure 3I).

Overall, these results suggest that the CIP system based on PYR1-ABI1 holds promising potential in the field of targeted cancer therapy.

Evolution of ABA-induced interaction of PYR1-ABI1 using PACE

While the PYR1-ABI1 interaction exhibits higher ABA response

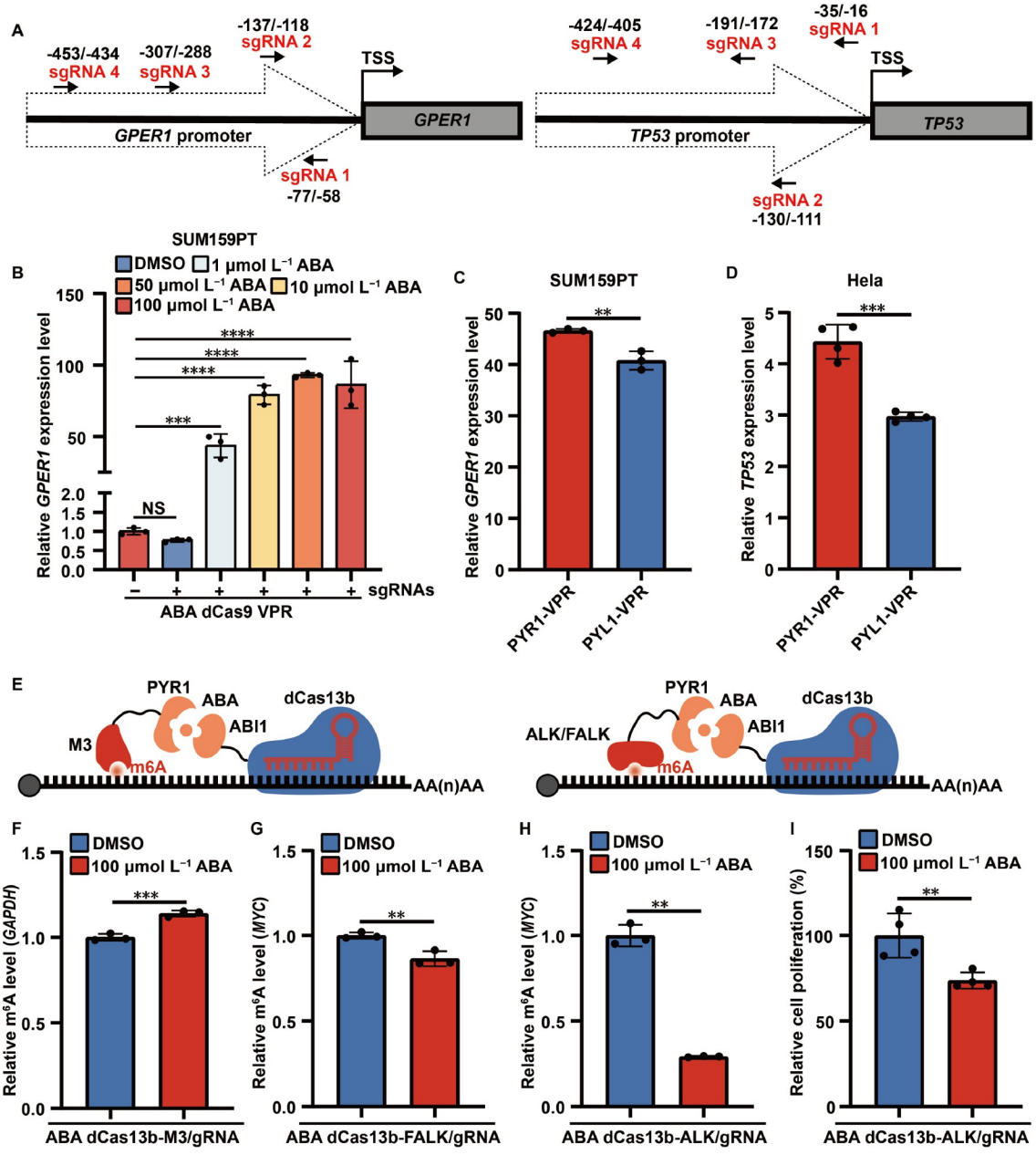

Figure 3. The regulation of endogenous genes at the transcriptional and post-transcriptional levels. A, Binding position (indicated by black arrows) of four gRNAs in the promoter of *GPER1* gene (left) or *TP53* gene (right). B, qRT-PCR analysis of mRNA expression level of *GPER1* in SUM159PT cells co-transfected with four *GPER1*-specific gRNA mix or pUC19 vector in ABA dCas9-VPR system. Transfected cells were treated with DMSO (0 μmol L^{-1}) or ABA (1, 10, 50, 100 μmol L^{-1}) for 24 h prior to RNA extraction. Cells co-transfected with ABA dCas9-VPR and pUC19 vector treated with 100 μmol L^{-1} ABA as the negative control. Data are normalized to negative control and presented as mean ±SD (n=3). NS, no significance; ***, P<0.001; ****, P<0.0001 (one-way ANOVA). C, qRT-PCR analysis of mRNA expression level of *GPER1* in SUM159PT cells. Cells expressing ABI1-dcas9 and the *GPER1*-specific gRNA mix were co-transfected with the plasmids expressing PYR1-VPR or PYL1-VPR, respectively. Transfected cells were treated with DMSO or 100 μmol L^{-1} ABA for 24 h prior to RNA extraction. Data are normalized to *GPER1* expression level of cells treated with DMSO and presented as mean±SD (n=3). **, P<0.01 (Two-tailed student's t-test). D, qRT-PCR analysis of mRNA expression level of *TP53* in HeLa cells. Cells expressing ABI1-dcas9 and the *TP53*-specific gRNA mix were co-transfected with the plasmids expressing PYR1-VPR or PYL1-VPR, respectively. Transfected cells were treated with DMSO or 100 μmol L^{-1} ABA for 24 h prior to RNA extraction. Data are normalized to *TP53* expression level of cells treated with DMSO and presented as mean±SD (n=3). ***, P<0.001(Two-tailed student's t-test). E, Schematic of ABA-induced RNA m^6A installation system (left) and ABA-induced RNA m^6A removal system (right). F, m^6A RIP-qPCR analysis of *GAPDH* mRNA in HEK293T cells co-transfected with the plasmids expressing ABI1-dCas13b-6×Flag, PYR1-M3-4×Myc and *GAPDH*-specific gRNA mix under the treatment of DMSO or 100 μmol L^{-1} ABA, respectively, for 48 h. Data are normalized to the m^6A level of *GAPDH* mRNA in cells treated with DMSO and presented as mean±SD (n=3). ***, P<0.001 (Two-tailed student's t-test). G, m^6A RIP-qPCR analysis of *MYC* mRNA in HeLa cells co-transfected with the plasmids expressing ABI1-dCas13b-6×Flag, PYR1-FALK-4×Myc and *MYC*-specific gRNA mix under the treatment of DMSO or 100 μmol L^{-1} ABA, respectively, for 48 h. Data are normalized to the m^6A level of *MYC* mRNA in cells treated with DMSO and presented as mean±SD (n=3). **, P<0.01 (Two-tailed student's t-test). H, m^6A RIP-qPCR analysis of *MYC* mRNA in HeLa cells co-transfected with the plasmids expressing ABI1-dCas13b-6×Flag, PYR1-ALK-4×Myc and *MYC*-specific gRNA mix under the treatment of DMSO or 100 μmol L^{-1} ABA, respectively, for 48 h. Data are normalized to the m^6A level of *MYC* mRNA in cells treated with DMSO and presented as mean±SD (n=3). **, P<0.01 (Two-tailed student's t-test). I, Proliferation of HeLa cells co-transfected with the plasmids expressing ABI1-dCas13b-6×Flag, PYR1-ALK-4×Myc and *MYC*-specific gRNA mix under the treatment of DMSO or 100 μmol L^{-1} ABA, respectively, for 48 h. Data are normalized to the A_{450} nm of cells treated with DMSO and presented as mean±SD (n=3). **, P<0.01 (Two-tailed student's t-test).

https://doi.org/10.1007/s11427-024-2707-9

intensity as a transcription activation tool than the PYL1-ABI1 interaction, it was unclear whether enhancing the interaction strength between PYR1 and ABI1 could further amplify this response. Before this study, PACE, known for its simplicity, ease of operation, and high efficiency as a protein-directed evolution tool, had not yet been implemented in the evolution of CIP. We believe that PACE holds promising potential for evolving the ABA-induced interaction of PYR1-ABI1. Therefore, we established a dedicated PACE system specifically designed for the evolution of ABA-induced PYR1-ABI1 interaction (Figure 4A).

To link the ABA-induced interaction of PYR1-ABI1 to phage proliferation, *PYR1* was subcloned into the selection phage (SP) plasmid and fused with rpoZ, while *ABI1* was subcloned into the accessory plasmid (AP) and fused with 434c . This configuration ensures that the transcription of *gene III* on the AP depends on the ABA-induced interaction of PYR1-ABI1. The protein III encoded by *gene III* is crucial for M13 phage proliferation and infection (Riechmann and Holliger, 1997). Generally, the more protein III is present, the more infectious progeny phages are produced (Rakonjac and Model, 1998). Therefore, there is a positive correlation between phage proliferation and the ABA-induced interaction of PYR1-ABI1. To ensure the PACE system runs smoothly, we continuously added arabinose and ABA to the lagoon using a syringe pump, aiming to induce the expression of the mutagenic genes on the mutagenic plasmid 6 (MP6) and ensure the sustained induction of the interaction of PYR1-ABI1 by ABA.

Prior to beginning PACE, we conducted a SP activity-dependent phage proliferation assay to determine whether the initial interaction capacity of PYR1-ABI1 induced by ABA could support phage survival under continuous flow conditions. The experimental results showed that the interaction between PYR1 and ABI1 led to an approximately 100-fold increase in phage proliferation in the absence of ABA. By contrast, under ABA induction, it increased approximately 1000-fold (Figure 4B). Typically, an overnight proliferation capacity of 100-1000 times is sufficient to begin PACE experiments (Miller et al., 2020a). These results indicate that the initial interaction capacity of PYR1-ABI1 induced by ABA can support the running of PACE systems.

During PACE, we took a sample from the lagoon every 12 h for phage titer determination and adjusted the flow rate as needed based on the phage proliferation status. The flow rate of the lagoon determines the selection pressure and is crucial for successful PACE runs. After 252 h of selection, the flow rate of the evolution pool reached 7 vol h^{-1}, and the phage titer was maintained at a high level (approximately 10^7 pfu mL^{-1}) (Figure 4D). This suggests that the phages likely acquire beneficial mutations to support their survival under high selection pressure. Through Sanger sequencing, we subsequently identified two mutation sites in PYR1, D100N, and E102V, which appeared at 156 h and continuing until 252 h (Figure 4C). These results indicate that the mutations at D100N and E102V likely enhance the ABA-induced interaction between PYR1 and ABI1.

Characterization of the evolved PYR1 mutant

We obtained the PYR1 mutant $PYR1^{D100N,E102V}$ (hereafter referred to as PYR1m) by PACE. To characterize the interaction between PYR1m and ABI1, we conducted the Split Luciferase assay to determine the kinetics of their interaction. The results showed that although PYR1m-ABI1 interaction under ABA induction was not as strong as that of PYR1-ABI1 and PYL1-ABI1 (Figure 5A), its ABA response intensity was the highest of the three (Figure 5B; Figure S8 in Supporting Information). A subsequent reporter gene activation experiment indicated that under ABA induction, the *Ren* activation level induced by PYR1m-VPR was higher than that induced by PYR1-VPR with similar expression levels of PYR1-VPR and PYR1m-VPR (Figure 5C; Figure S5 in Supporting Information). Further experiments on endogenous gene transcription activation also showed that the transcription activation level of *GPER1* induced by PYR1m-VPR was higher than that of PYR1-VPR (Figure 5D and F) in both HEK293T cells and SUM159PT cells under ABA induction. These results suggest that the transcription activation tool based on PYR1m-ABI1 has a higher ABA response intensity than that based on PYR1-ABI1.

We subsequently compared the efficiency of PYR1, PYL1, and PYR1m in ABA-induced RNA m^6A modification editing. As shown in Figure 5F, under ABA induction, PYR1-ALK, PYL1-ALK, and PYR1m-ALK all significantly reduced relative m^6A level (the ratio of the m^6A level under ABA treatment to that under DMSO treatment) of *MYC* gene. Unexpectedly, while PYR1-ALK exhibited the strongest m^6A removal capability of the three, PYR1m-ALK showed the lowest m^6A removal capability. With similar expression levels of PYR1-ALK, PYL1-ALK, and PYR1m-ALK in HeLa cells (Figure S9 in Supporting Information), the ABA-induced m^6A removal tool based on PYR1-ABI1 has the highest ABA response intensity. Contrary to the transcription activation system based on PYR1m-ABI1, which exhibits the highest ABA response intensity, the m^6A removal tool based on PYR1m-ABI1 demonstrates the lowest ABA response intensity. This discrepancy may arise from differences in the mechanisms governing transcription and m^6A modifications (Flamand et al., 2023).

DISSCUSION

In recent years, many studies have expanded on the application of the ABA-based CIP system, such as inducing histone modifications, inducing installation and removal of RNA m^6A modification, and even modifying the activating ligand (Chen et al., 2017; Shi et al., 2022; Park et al., 2023). However, before this study, modification of the system itself to obtain an ABA-based CIP system with stronger ABA response intensity had not yet to be attempted. We speculate that the ABA responsiveness of CIP may be related to the protein interaction intensity. *In vitro* evidence has demonstrated that the interaction between PYR1 and ABI1 is stronger than that between PYL1 and ABI1 (Nemoto et al., 2018). Therefore, we aimed to characterize the interaction between PYR1 and ABI1 using Split Luciferase assay in HEK293T cells. We found that the interaction intensity of PYR1-ABI1, under both low and high concentrations of ABA, was lower than that of PYL1-ABI1, which may be attributed to differences between *in vivo* and *in vitro* conditions. However, when ABA was not added, the interaction intensity between PYR1 and ABI1 was lower (Figure 2A), which was consistent with our expectations. We discovered that while the PYR1-ABI1 pair has a lower basal interaction than PYL1-ABI1 without ABA, it has a stronger response interaction after the addition of ABA (i.e., higher Luc^{+ABA}/Luc^{-ABA} values). This suggests that the CIP system based on PYR1-ABI1 is more inducible and has more

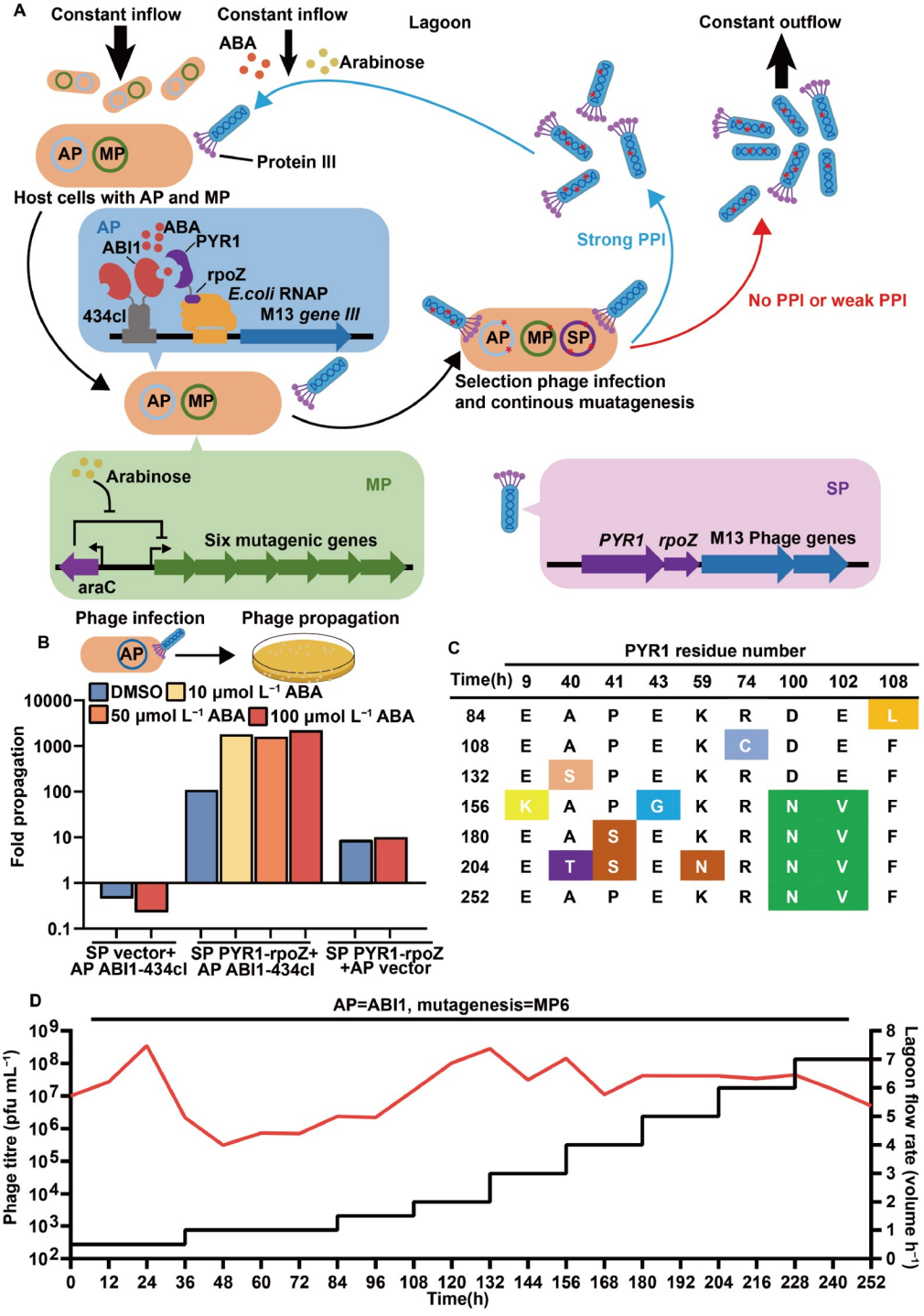

Figure 4. Evolution of ABA-induced interaction between PYR1 and ABI1 using PACE. A, Overview of the PACE. In our PACE, the host *E. coli* cell carries two plasmid: accessory plasmid (AP ABI1-434cI) and MP6. M13 *gene III* is an essential gene for the infection and propagation of M13 phage. To link the transcription of *gene III* to the activity of interest, *gene III* is deleted from the SP and replaced with *PYR1-rpoZ*, and the *gene III* is cloned into AP. Then the transcription of *gene III* is dependent on the ABA-induced interaction between ABI1-434cI from AP and PYR1-RpoZ from SP. MP6 contains six mutagenic genes which are under the control of the arabinose operon and elevate the mutagenic rate during DNA replication. During PACE, selection phages were continuously diluted by the constant influx of the host *E. coli* cells in the lagoon. Mutations (indicated as red stars) accumulated in the phages that could result in stronger PYR1-ABI1 interactions, allowing for the production of more protein III. Consequently, a large number of infectious progeny phages were generated. Conversely, when mutations in the accumulating phages led to no or weak interactions with PYR1-ABI1, the phages would flow out of the lagoon. PPI: protein-protein interaction. RpoZ: the omega subunit of *E. coli* RNA polymerase, which can function as a transcriptional activation domain (Badran et al., 2016). 434cI: the 434 phage cI repressor, which can function as a DNA-binding domain that binds to the specific region upstream of *gene III* in AP (Badran et al., 2016). B, Propagation of empty phage (SP vector), PYR1-rpoZ phage (SP PYR1-rpoZ) in host *E. coli* cells carried indicated AP plasmid under the treatment of DMSO or ABA (10, 50, 100 μmol L^{-1}). Propagation of empty phage in host *E. coli* cells carried AP ABI1-434cI and propagation of PYR1-rpoZ phage in host *E. coli* cells carried AP vector as the negative control. C, Oligotyping analysis of lagoon samples at indicated timepoint using Sanger sequencing during PACE. Each color represents one oligotype. Mutations in each oligotype of PYR1 are shown in the table. D, The phage titers and the lagoon flow rate at indicated timepoint during PACE were shown.

https://doi.org/10.1007/s11427-024-2707-9

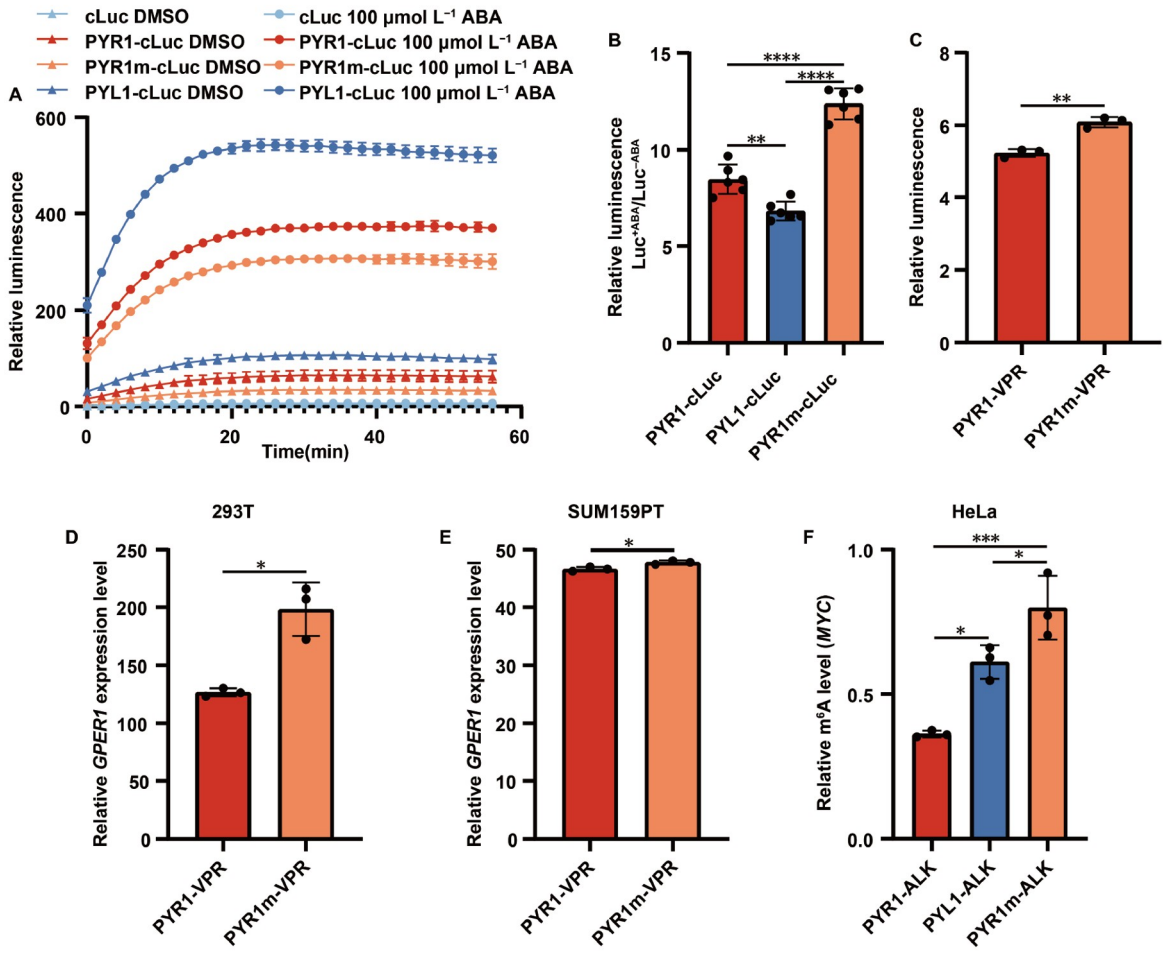

Figure 5. Characterization of the evolved PYR1 variant. A, Bioluminescence analysis of HEK293T cells co-transfected with the plasmids expressing ABI1-nLuc and cLuc, PYR1-cLuc, PYR1m-cLuc or PYL1-cLuc, respectively. Transfected cells were treated with DMSO or 100 μmol L^{-1} ABA for 24 h prior to bioluminescence measurement. The bioluminescence was collected every two minutes. Data are normalized to the bioluminescence of cells transfected with ABI1-nLuc and cLuc under the treatment of 100 μmol L^{-1} ABA at the first timepoint and presented as mean±SD (n=6). B, Relative bioluminescence analysis of HEK293T cells co-transfected with the plasmids expressing ABI1-nLuc and PYR1-cLuc, PYR1m-cLuc or PYL1-cLuc under 100 μmol L^{-1} ABA treatment, respectively. The bioluminescence at the first time point are shown. Data are normalized to the bioluminescence of cells treated with DMSO and presented as mean±SD (n=6). **, P<0.01; ****, P<0.0001 (one-way ANOVA). C, HEK293T cells expressing pSV40-Ren, ABI1-dCas9, and sgRNA SV40 were transfected with the plasmid expressing PYR1-VPR or PYR1m-VPR, respectively. Transfected cells were treated with DMSO (0 μmol L^{-1}) or 100 μmol L^{-1} ABA for 24 h prior to bioluminescence measurement. Data are normalized to the bioluminescence of cells treated with DMSO and presented as mean±SD (n=3). **, P<0.01 (Two-tailed student's t-test). D, qRT-PCR analysis of mRNA expression level of *GPER1* in HEK293T cells. Cells expressing ABI1-dcas9 and *GPER1*-specific gRNA mix were co-transfected with the plasmids expressing PYR1-VPR or PYL1-VPR, respectively. Transfected cells were treated with DMSO or 100 μmol L^{-1} ABA for 24 h prior to RNA extraction. Data are normalized to *GPER1* expression level of cells treated with DMSO and presented as mean±SD (n=3). *, P<0.05 (Two-tailed student's t-test). E, qRT-PCR analysis of mRNA expression level of *GPER1* in SUM159PT cells. Cells expressing ABI1-dcas9 and *GPER1*-specific gRNA mix were co-transfected with the plasmids expressing PYR1-VPR or PYL1-VPR, respectively. Transfected cells were treated with DMSO or 100 μmol L^{-1} ABA for 24 h prior to RNA extraction. Data are normalized to *GPER1* expression level of cells treated with DMSO and presented as mean±SD (n=3). *, P<0.05 (Two-tailed student's t-test). F, m^6A RIP-qPCR analysis of *MYC* mRNA in HeLa cells expressing ABI1-dCas13b-6×Flag and *MYC*-specific gRNA mix co-transfected with the plasmids expressing PYR1-ALK-4×Myc, PYL1-ALK-4×Myc or PYR1m-ALK-4×Myc under the treatment of DMSO or 100 μmol L^{-1} ABA for 48 h, respectively. Data are normalized to the m^6A level of *MYC* mRNA in cells treated with DMSO and presented as mean±SD (n=3). *, P<0.05; ***, P<0.001 (One way ANOVA).

promising applications. Consistent with our speculations, the degree to which the transcriptional activation system based on PYR1-ABI1 activates genes inhibiting cancer cell proliferation is significantly higher than that of PYL1-ABI1 in both SUM159PT and HeLa cells. Previous research indicates that the auxin-inducible degron (AID) system based on AtAFB2 has a lower basal degradation level than that based on *Oryza sativa* TIR1 (Li et al., 2019). In other words, the AID system based on AtAFB2 exhibits a stronger response to auxin. Differential hormone responsiveness may arise from distinct receptors for the same hormone. Therefore, we hypothesize that structural differences between PYR1 and PYL1 proteins contribute to the higher ABA response intensity observed in the PYR1-ABI1 pair. Previous studies applied the PYL1-ABI1 interaction to regulate RNA m^6A levels, and we recapitulated this the regulatory role of PYR1-ABI1 interaction at the RNA m^6A level. Similar to the ABA-induced transcriptional activation system based on PYR1-ABI1, the ABA-induced m^6A removal system based on PYR1-ABI1 also exhibits higher ABA responsiveness compared with that based on PYL1-ABI1. This indicates that the PYR1-ABI1 pair is a more feasible substitution within the original application scope of the PYL1-ABI1 pair (Shi et al., 2022). To improve upon the ABA-based CIP system, we employed PACE to conduct directed evolution on PYR1, screening for PYR1 mutants that would

exhibit enhanced performance during transcriptional activation. Prior to this study, researchers have also screened PYR1 mutants to address various challenges, such as creating constitutively active receptors (Mosquna et al., 2011) and developing biosensors (Beltrán et al., 2022). These mutants were obtained by site-saturation mutagenesis, followed by extensive experimental screening. Undoubtedly, compared with site-saturation mutagenesis, PACE offers significant advantages, including minimal manual intervention, simplicity, and high efficiency (Esvelt et al., 2011; Morrison et al., 2020). The foundation of PACE for evolving protein-protein interactions is based on the *Escherichia coli* two-hybrid system (Dove and Hochschild, 1998; Badran et al., 2016), which activates the transcription of *gene III* through protein-protein interaction, thereby linking protein interaction activity with phage proliferation activity. This strategy is similar to the ABA-induced transcriptional activation system established based on PYR1-ABI1, making PACE particularly suitable for evolving ABA-induced protein interactions or other CIP systems.

Unlike current PACE protocols (Badran et al., 2016), we placed RpoZ and 434cI at the C-terminus rather than at the N-terminus of the fusion protein, designing a protein fusion expression strategy for PYR1-RpoZ and ABI1-434cI. Although studies have shown that RpoZ at the C-terminus of the fusion protein may affect the recruitment of other components of RNA polymerase (Dove and Hochschild, 1998), phage proliferation experiments found that the PYR1-RpoZ/ABI1-434cI pair can enable phage proliferation and have an ABA response, indicating that *gene III* can be normally activated upon ABA induction.

The evolved PYR1m demonstrated enhanced activity in the transcriptional activation system together with ABI1 in host *E. coli* cells, as evidenced by increased phage proliferation (Figure 4C). However, Split Luciferase assay in HEK293T cells indicated that the strength of the interaction between PYR1m and ABI1 did not surpass that of PYR1-ABI1. Nevertheless, the ABA response intensity of PYR1m-ABI1 interaction was stronger than that of PYR1-ABI1 interaction, and the basal interaction of PYR1m-ABI1 was weaker in the absence of ABA (Figure 5A and B). Consistent with the evolutionary results, the transcriptional activation tool based on PYR1m-ABI1 also exhibited improved transcriptional activation in both HEK293T cells and SUM195PT cells (Figure 5C–E). Collectively, the two mutation sites, D100N and E102V, result in a weaker basal interaction between PYR1m and ABI1, thereby leading to an enhanced ABA response intensity in terms of interaction and transcriptional activation. This phenomenon is analogous to the distinct auxin responses in AID system based on different auxin receptors (Li et al., 2019). However, the m^{6}A removal system based on PYR1m-ABI1 demonstrates a lower ABA response intensity than that based on PYR1-ABI1 and PYL1-ABI1, which may be attributed to the complexity of m^{6}A modification and recognition mechanisms (Flamand et al., 2023). Considering D100N and E102V are not located within the ABA-binding pocket of PYR1 (Rodriguez et al., 2019), further protein structural analysis is required to elucidate the specific mechanisms underlying the reduced basal interaction of PYR1m-ABI1.

The engineered PYR1m-ABI1 enhanced the advantages of the ABA-based CIP system. This modification strategy can be applied to other plant hormone-based CIP systems, such as GID1-GAI (Bao et al., 2017) and IAA17-OsTIR1 (Li et al., 2019). Furthermore, this strategy can be extended to other proximity systems, including light-induced protein proximity, small molecule-nanobody conjugate induced proximity, and others (Klewer and Wu, 2019; Sun et al., 2023).

MATERIALS AND METHODS

Cell culture

HEK-293T cells (ATCC, ATCC®CRL-11268™) and HeLa cells (ATCC, CRM-CCL-2 ™) were cultured in DMEM (VivaCell, C3113-0500) supplemented with 10 % (v/v) FBS (TOCYTO, UT82901), 100 U mL^{-1} penicillin, and 100 mg mL^{-1} streptomycin (Hyclone, SV30010). Triple Negative subtype of breast cancer SUM159PT cells (MeisenCTCC, CTCC-400-0116) were cultured in RPMI 1640 (MeisenCTCC, CTCC-002-003) supplemented with 10% (v/v) FBS (TOCYTO, UT82901), 100 U mL^{-1} penicillin, and 100 mg mL^{-1} streptomycin (Hyclone, SV30010). HEK-293T cells, HeLa cells and SUM159PT cells were cultured in humidified 5% (v/v) CO_2 in air, at 37°C.

Bacteria strains

E. coli S2060 cells (Addgene, #105064) were purchased from Addgene. *E. coli* S2208 cells: S2060 cells transformed with pJC175e (Addgene, #79219), which produces functional pIII in response to phage infection.

sgRNA design

sgRNAs sequences for *Luc*, *Ren*, *GPER1* and *TP53* activation were identified using Genscript CRISPR sgRNA Design Tool (https://www.genscript.com.cn/gRNA-design-tool.html). sgRNAs sequences for *TTN* activation described by Chavez et al. were used (Chavez et al., 2015). sgRNAs for *Luc* or *Ren* activation were selected to bind between 1 to 500bp upstream of ATG. sgRNAs for *GPER1* and *TP53* activation were selected to bind between 1 to 500 bp upstream of the transcriptional start site. SgRNA targets *GAPDH* mRNA described by David R.Liu was used (Wilson et al., 2020). SgRNA targets *MYC* mRNA described by Jiexin Li at al. was used (Li et al., 2020). All sgRNA sequences were listed in Table S1 and S2.

Plasmids construction

Full-length ABI1, PYR1 and PYL1 were amplified from the *Arabidopsis thaliana* cDNA library. PYR1 mutant was obtained by Fusion-PCR. DCas9 and VPR (VP64, p65, and Rta) were synthesized by Sangon (Sangon Biotechnology Co., Ltd, Shanghai, China). dCas13b was amplified from pC0054-CMV-dPspCas13b-longlinker-ADAR2DD (E488Q/T375G) (Addgene, #103870). All the genes were subcloned into pCI (neo) (Promega, E1841). For BiFC assay, N terminus of YFP (nYFP) was fused with ABI1 via a flexible $(GGGS)_3$ linker, C terminus of CFP (cCFP) was fused with PYR1 via a flexible $(GGGS)_3$ linker. For Co-IP assay, ABI1 was fused with N-terminal 6×Flag tag, PYR1 was fused with N-terminal GFP tag via a flexible $(GGGS)_3$ linker. For Split Luciferase assay, ABI1 was fused with N terminus of Luc (nLuc) via a flexible $(GGGS)_3$ linker, PYR1 was fused with C terminus of Luc (cLuc) via a flexible $(GGGS)_3$ linker. For Luc/Ren reporter gene activation assay, pNL2.2 FT G::Luc and pNL2.2 pSV40::Ren were used, dCas9 was fused with VPR

https://doi.org/10.1007/s11427-024-2707-9

via SV40 NLS linker (PKKKRKV). For ABA Split dCas9 VPR, dCas9N1-535 was fused with PYR1 via a flexible $(GGGS)_3$ linker, ABI1 was fused with dCas9C536-1368-VPR via a flexible $(GGGS)_3$ linker. For ABA dCas9 VPR, ABI1 was fused with dCas9 via a flexible $(GGGS)_3$ linker, PYR1 or PYL1 was fused with VPR via SV40 NLS linker (PKKKRKV). For ABA-inducible m^{6}A writing system, ABI1 was fused with C-terminal 6×Flag tagged dCas13b via a $(GGGS)_3$-$(NLS)_3$ linker, PYR1 was fused with C-terminal 4×Myc tagged Mettl3$^{273–580}$ via a $(GGGS)_3$-$(NLS)_3$ linker. For ABA-inducible m^{6}A erasing system, ABI1 was fused with C-terminal 6×Flag tagged dCas13b via a $(GGGS)_3$-NES linker, PYR1 was fused with C-terminal 4×Myc tagged FTO$^{36–325}$ or ALKBH5$^{66–292}$ via a $(GGGS)_3$-NES linker. Cas13 guide RNAs were T4 ligated into pC0043-PspCas13b-crRNA (Addgene, #103854). For dCas9 sgRNAs expression, each sgRNA driven by a human U6 promoter was subcloned into the pUC19 vector.

To generate SP PYR1-rpoZ used in PACE, *PYR1-linker-rpoZ* was subcloned into SP098. To generate AP ABI1-434cI, *ABI1-linker-434cI* was subcloned into pAB107a (Addgene, #79218). Linker used here was $(GGGS)_3$. MP6 (Addgene, #69669) was purchased from Addgene.

PEI-Max-based transient transfection

HEK-293T cells, HeLa cells or SUM159PT cells were seeded in a 6-well plate (Bioland, CCP06-006) to reach 70%–90% confluency before the transfection. Each well was transfected with 8 μL 1 mg mL^{-1} PEI-Max (Polysciences, Inc) in 150 μL Opti-MEM (Gbico, 11058-021) with 4 μg total plasmid DNA. 4 μg total plasmid DNA was diluted with 150 μL Opti-MEM, and then 8 μL 1 mg mL^{-1} PEI-Max was added into the Opti-MEM-DNA mixture. After incubation at RT for 5 min, the mixture was added into the cells gently and then transfected cells were incubated in humidified 5% (v/v) CO_2 in air, at 37°C.

ABA induction experiments

Transfected cells were incubated in a cell culture incubator for 24 h and then treated with DMSO (final concentration 0.1%) or different concentrations of ABA for another 24 h (Co-IP, BiFC, Split-Luc, gene activation assay and CCK8 assay) or 48 h (m^{6}A modification editing). ABA was dissolved in 100% DMSO to prepare a number of 1000-fold stock solutions (1, 10, 50, 100 mmol L^{-1}), so the control group received an equivalent volume of 100% DMSO. Both ABA and DMSO were added to cell culture medium in a ratio of 1 to 1000.

Co-immunoprecipitation (Co-IP) assay and immunoblot

Transfected HEK-293T cells were incubated in humidified 5% (v/v) CO2 in air, at 37°C. After 24 h, cells were treated with 100 μmol L^{-1} ABA (Sigma, A1049-250MG) or DMSO (Sigma, D2438) for another 24 h. Then, cells were washed with PBS (VivaCell, C3590-0500) and detached by TrypLE TM Express (Gbico, 12605-028), the detached cells were collected by centrifuge at 800×*g* for 5 min and lysed by Pierce IP Lysis Buffer (Pierce, 87787) supplemented with 1×EDTA-free Protease Inhibitor Cocktail Tablets (Pierce, A32965). After incubation on ice for 10 min, the lysate was centrifuged 12000×*g* for 10 min. With 50 μL supernatant as the input sample, the remaining supernatant was incubated with 20 μL GFP-Trap beads for 2 h at 4°C on a rotator. Beads were washed 5 times by wash buffer (25 mmol L^{-1} Tris-HCl pH 7.4, 150 mmol L^{-1} NaCl, 1 mmol L^{-1} EDTA, 0.1% NP-40 and 5% Glycerol) and denatured by mixing thoroughly with 40 μL 4×SDS sample buffer and heating at 95°C for 5 min. Samples were analyzed on 10% SDS-polyacrylamide gel electrophoresis and transferred to nitrocellulose transfer membranes (Merck Millipore, HATF00010). The primary antibodies are anti-GFP (1:5000; MBL, 598) and anti-DDDDK (1:5000; MBL, M185-3L).

BiFC assay

HEK-293T cells were cultured in 20 mm glass bottom cell culture dish (Bioland, CDG35-20) and transfected with desired vectors using PEI-Max. Transfected cells were incubated in humidified 5% (v/v) CO2 in air, at 37°C. After 24 h, cells were treated with 100 μmol L^{-1} ABA or DMSO for another 24 h. Then, cells were observed under a confocal laser scanning Nikon Ti2 microscope. Fluorescent signals were detected at 514 nm for YFP channel.

Split-luciferase assay

HEK-293T cells were transfected with desired vectors using PEI-Max. Transfected cells were incubated in humidified 5% (v/v) CO_2 in air, at 37°C. After 24 h, cells were treated with 100 μmol L^{-1} ABA or DMSO for another 24 h. Then, cells were washed with PBS (pH 7.2) and coated with 10 mL DMEM without FBS medium, at 37°C, 5% CO_2 incubated for 1 h. Cells were resuspended with 1 mL DMEM (without Phenol red) with 10% FBS and 1 mmol L^{-1} Luciferin, 1 mmol L^{-1} Forskolin, 200 nmol L^{-1} Dex. After incubated in the dark for 5 min, the luminescence was detected by a EnSight™ Multimode Microplate Reader (PerkinElmer).

Luc/Ren reporter gene activation assay

HEK-293T cells were transfected with desired vectors using PEI-Max. Transfected cells were incubated in humidified 5% (v/v) CO_2 in air, at 37°C. After 24 h, cells were treated with 100 μmol L^{-1} ABA or DMSO for another 24 h. Then, the experiment was performed according to the user manual for Dual-Luciferase® Reporter Assay System kit (Promega, E1910).

CCK8 assay

Transfected cells were cultured in a 96-well plate with 4000 cells in each well for 24 h. Then the cells were treated with DMSO or 100 μmol L^{-1} ABA. After 48 h, 10 μL CCK8 reagent (LABLEAD Inc., CK001) was added into each well and the plate was continued to be cultured for 4 h. The optical density absorbance at the wavelength of 450 nm was measured by microplate reader to detect cell proliferation.

Gene-specific m^{6}A RIP-qPCR

20 μL Protein A/G Magnetic Beads (Sigma-Aldrich, 16-663) were incubated with 1 μg m^{6}A antibody (SYSY, 202003) in 500 μL IP buffer (150 mmol L^{-1} NaCl, 0.1% NP-40, 10 mmol L^{-1} Tris-HCl pH 7.4, 100 U RNase inhibitor) at 4°C for 3 h on a rotator. Total RNA was isolated using TransZol Up Plus RNA Kit (TransGen Biotech, ER501-01-V2). With 500 ng RNA

kept as an input sample, 200 μg RNA were added into m^{6}A antibody-conjugated Protein A/G Magnetic Beads at 4°C for another 3 h on a rotator. After washing by IP buffer with RNase inhibitors four times, the bound RNA was isolated from the washed Protein A/G Magnetic Beads using TRIzol reagent according to the manufacturer's protocol. The same amount of the IP RNA or input RNA from each sample was reverse-transcribed into cDNA using First-strand cDNA Synthesis Mix (LABLEAD Inc., F0202) and subjected to qRT-PCR. The relative m^{6}A level of genes were calculated by m^{6}A level (m^{6}A IP) normalized using the expression of each gene (Input).

qRT-PCR analysis

Total RNA was isolated from transfected cells according to the user manual for RNAprep Pure Cell/Bacteria Kit (TIANGEN, DP430). RNA purity and concentration were evaluated by NanoPhotometer® N60 (IMPLEN). 2 μg purified total RNA per sample was used as a template for cDNA synthesis using the First-strand cDNA Synthesis Mix (LABLEAD Inc., F0202), the experiment was performed according to the user manual. qRT-PCR was carried out on the CFX96 Real-Time PCR Detection System (BIORAD) using the GoTaq® qPCR Master Mix (Promega, A6001) according to the manufacturer's protocol. Relative quantification of gene expression was carried out according to the comparative (ΔΔ) Ct method, with *GAPDH* as housekeeping genes. All primer sequences were listed in Table S3.

SP activity-independent phage plaque assay

Dilute S2208 cells cultured overnight 100-fold into 2×YT media supplemented with 100 μg mL^{-1} ampicillin and grow at 37°C in a shaker to A_{600} of 0.4–0.6. The filtered phage sample were diluted serially in water in three 100-fold increments (undiluted, 10^2-, 10^4-, 10^6- diluted). 10 μL of each diluted phage was added into each of four tubes containing 100 μL S2208 cells. Then 800 μL warm (50–60°C) 2×YT agar (0.7%) was added into each tube and mix well by pipetting, and plate onto 4-sector LB agar (1.5%) plates. The plates were incubated at 37°C overnight prior to counting phage plaque.

SP activity-dependent phage propagation assay

S2060 cells were transformed with AP ABI1-434cI. Dilute cells cultured overnight 100-fold into 2×YT media supplemented with 100 μg mL^{-1} ampicillin and grow at 37°C in a shaker to A_{600} of 0.4–0.6. The cells were infected with SP PYR1-rpoZ phage at a starting titre of 10^6 pfu mL^{-1} and grow at 37°C in a shaker for another 5–8 h with DMSO or ABA treatment. Pellet the cells by centrifuging at 12000g for 5 min and filter the supernatant using a 0.22 μm filter to remove the residual cells. The phage titer was determined using an activity-independent phage plaque assay and the fold propagation was calculated.

PACE

PACE was conducted by following David. R Liu's protocol (Miller et al., 2020a). Briefly, to prepare the phage stock, SP PYR1 phage was plaqued on S2208. A single plaque was picked into 1 mL S2208 (A_{600}=0.4–0.6) and incubated at 37°C in a shaker for another 5–8 h. Phage was stocked at 4°C after the titer was determined using an activity-independent phage plaque assay and stocked at 4°C. To prepare the host *E. coli* cell, S2060 cells co-transformed with AP ABI1-434cI and MP6 were plated on 1.5% LB agar supplemented with 100 μg mL^{-1} ampicillin, 40 μg mL^{-1} chloramphenicol and 100 mmol L^{-1} glucose. After overnight incubation at 37°C in a incubator, a single clone was picked into 1 mL DRM and incubated at 37°C in a shaker for 12–16 h. The S2060 cells carried AP and MP was diluted 100-fold into 80 mL DRM and incubated at 37°C in a shaker to A_{600} of 0.6–0.8. 17 mL prepared S2060 cells were added into each of two lagoon and then infected with SP PYR1-rpoZ phage at a starting titer of 10^6 pfu mL^{-1}. The remaining prepared S2060 cells were added into the chemostat supplemented with fresh DRM. The chemostat culture was maintained at 80 mL and grown at a dilution rate of 1 volume per hour in the beginning. The lagoon culture flowing from the chemostat was maintained at 17 mL and grown at a dilution rate of 0.5 volume per hour in the beginning. The dilution rate of the chemostat and the lagoon needed to be adjusted at any time according to the phage titers of the lagoon during PACE. To ensure the mutagenic rate, 250 mmol L^{-1} arabinose were added into the lagoon at a rate of 1 mL h^{-1} by a syringe pump. Phage samples were taken from the lagoon every 12 h and determined titers using an activity-independent phage plaque assay. Whether or not to send phage samples for sanger sequencing depends on the change of phage titers during PACE.

Sanger sequencing of phage PYR1 mutants

An activity-independent phage plaque assay was conducted to determine phage titers of phage samples taken from the lagoon and isolate single plaque. PCR was performed with 2×NG PCR Master Mix (HLINGENE, NG001M) using following primers: AB1792F (TAATGGAAACTTCCTCATGAAAAAGTCTTTAG) and AB1396R (ACAGAGAGAATAACATAAAAACAGG-GAAGC). To provide the PCR template, phage plaques were briefly touched with pipette tips, which were then dipped into PCR reactions. The PCR products were sequenced with gVIII197F (GAAATTCACCTCGAAAGCAA).

Compliance and ethics

The authors declare that the research was conducted in the absence of any commercial or financial relationships that could be construed as a potential conflict of interest.

Acknowledgement

This work was supported by grants from China Postdoctoral Science Foundation (2022TQ0120, 2022M721320), the Science and Technology Research Project of the Education Department of Jilin Province, China (JJKH20221036KJ), the Open Project of State Key Laboratory of Supramolecular Structure and Materials (sklssm2023033) and Natural Science Foundation of Jilin Province (20240305059YY). We thank LetPub (www.letpub.com) for its linguistic assistance during the preparation of this manuscript.

Supporting information

The supporting information is available online at https://doi.org/10.1007/s11427-024-2707-9. The supporting materials are published as submitted, without typesetting or editing. The responsibility for scientific accuracy and content remains entirely with the authors.

References

Badran, A.H., Guzov, V.M., Huai, Q., Kemp, M.M., Vishwanath, P., Kain, W., Nance, A.M., Evdokimov, A., Moshiri, F., Turner, K.H., et al. (2016). Continuous evolution of *Bacillus thuringiensis* toxins overcomes insect resistance. Nature 533, 58–63.

Bao, Z., Jain, S., Jaroenpuntaruk, V., and Zhao, H. (2017). Orthogonal genetic regulation in human cells using chemically induced CRISPR/Cas9 activators. ACS Synth Biol 6, 686–693.

Beltrán, J., Steiner, P.J., Bedewitz, M., Wei, S., Peterson, F.C., Li, Z., Hughes, B.E.,

Hartley, Z., Robertson, N.R., Medina-Cucurella, A.V., et al. (2022). Rapid biosensor development using plant hormone receptors as reprogrammable scaffolds. Nat Biotechnol 40, 1855–1861.
Blum, T.R., Liu, H., Packer, M.S., Xiong, X., Lee, P.G., Zhang, S., Richter, M., Minasov, G., Satchell, K.J.F., Dong, M., et al. (2021). Phage-assisted evolution of botulinum neurotoxin proteases with reprogrammed specificity. Science 371, 803–810.
Bottone, S., Joliot, O., Cakil, Z.V., El Hajji, L., Rakotoarison, L.M., Boncompain, G., Perez, F., and Gautier, A. (2023). A fluorogenic chemically induced dimerization technology for controlling, imaging and sensing protein proximity. Nat Methods 20, 1553–1562.
Cao, L., Liu, X., Zheng, B., Xing, C., and Liu, J. (2022). Role of K63-linked ubiquitination in cancer. Cell Death Discov 8, 410.
Chavez, A., Scheiman, J., Vora, S., Pruitt, B.W., Tuttle, M., P R Iyer, E., Lin, S., Kiani, S., Guzman, C.D., Wiegand, D.J., et al. (2015). Highly efficient Cas9-mediated transcriptional programming. Nat Methods 12, 326–328.
Chavez, A., Tuttle, M., Pruitt, B.W., Ewen-Campen, B., Chari, R., Ter-Ovanesyan, D., Haque, S.J., Cecchi, R.J., Kowal, E.J.K., Buchthal, J., et al. (2016). Comparison of Cas9 activators in multiple species. Nat Methods 13, 563–567.
Chen, T., Gao, D., Zhang, R., Zeng, G., Yan, H., Lim, E., and Liang, F.S. (2017). Chemically controlled epigenome editing through an inducible dCas9 system. J Am Chem Soc 139, 11337–11340.
Cox, D.B.T., Gootenberg, J.S., Abudayyeh, O.O., Franklin, B., Kellner, M.J., Joung, J., and Zhang, F. (2017). RNA editing with CRISPR-Cas13. Science 358, 1019–1027.
Cutler, S.R., Rodriguez, P.L., Finkelstein, R.R., and Abrams, S.R. (2010). Abscisic acid: emergence of a core signaling network. Annu Rev Plant Biol 61, 651–679.
Daniel, K., Icha, J., Horenburg, C., Müller, D., Norden, C., and Mansfeld, J. (2018). Conditional control of fluorescent protein degradation by an auxin-dependent nanobody. Nat Commun 9, 3297.
Deng, L.J., Deng, W.Q., Fan, S.R., Chen, M.F., Qi, M., Lyu, W.Y., Qi, Q., Tiwari, A.K., Chen, J.X., Zhang, D.M., et al. (2022). m^{6}A modification: recent advances, anticancer targeted drug discovery and beyond. Mol Canc 21, 52.
Doman, J.L., Pandey, S., Neugebauer, M.E., An, M., Davis, J.R., Randolph, P.B., McElroy, A., Gao, X.D., Raguram, A., Richter, M.F., et al. (2023). Phage-assisted evolution and protein engineering yield compact, efficient prime editors. Cell 186, 3983–4002.e26.
Dove, S.L., and Hochschild, A. (1998). Conversion of the Omega subunit of *Escherichia coli* RNA polymerase into a transcriptional activator or an activation target. Genes Dev 12, 745–754.
Esvelt, K.M., Carlson, J.C., and Liu, D.R. (2011). A system for the continuous directed evolution of biomolecules. Nature 472, 499–503.
Feng, S., Laketa, V., Stein, F., Rutkowska, A., MacNamara, A., Depner, S., Klingmüller, U., Saez-Rodriguez, J., and Schultz, C. (2014). A rapidly reversible chemical dimerizer system to study lipid signaling in living cells. Angew Chem Int Ed 53, 6720–6723.
Flamand, M.N., Tegowski, M., and Meyer, K.D. (2023). The proteins of mRNA modification: writers, readers, and erasers. Annu Rev Biochem 92, 145–173.
Gao, Y., Xiong, X., Wong, S., Charles, E.J., Lim, W.A., and Qi, L.S. (2016). Complex transcriptional modulation with orthogonal and inducible dCas9 regulators. Nat Methods 13, 1043–1049.
Gourisankar, S., Krokhotin, A., Ji, W., Liu, X., Chang, C.Y., Kim, S.H., Li, Z., Wenderski, W., Simanauskaite, J.M., Yang, H., et al. (2023). Rewiring cancer drivers to activate apoptosis. Nature 620, 417–425.
Hernandez-Candia, C.N., Brady, B.R., Harrison, E., and Tucker, C.L. (2024). A platform to induce and mature biomolecular condensates using chemicals and light. Nat Chem Biol 20, 452–462.
Hu, J.H., Miller, S.M., Geurts, M.H., Tang, W., Chen, L., Sun, N., Zeina, C.M., Gao, X., Rees, H.A., Lin, Z., et al. (2018). Evolved Cas9 variants with broad PAM compatibility and high DNA specificity. Nature 556, 57–63.
Ke, X., and Shen, L. (2017). Molecular targeted therapy of cancer: The progress and future prospect. Front Lab Med 1, 69–75.
Klewer, L., and Wu, Y.W. (2019). Light-induced dimerization approaches to control cellular processes. Chem Eur J 25, 12452–12463.
Li, S., Prasanna, X., Salo, V.T., Vattulainen, I., and Ikonen, E. (2019). An efficient auxin-inducible degron system with low basal degradation in human cells. Nat Methods 16, 866–869.
Liang, F.S., Ho, W.Q., and Crabtree, G.R. (2011). Engineering the ABA plant stress pathway for regulation of induced proximity. Sci Signal 4, rs2.
Liang, Y., Lu, Q., Li, W., Zhang, D., Zhang, F., Zou, Q., Chen, L., Tong, Y., Liu, M., Wang, S., et al. (2021). Reactivation of tumour suppressor in breast cancer by enhancer switching through NamiRNA network. Nucleic Acids Res 49, 8556–8572.
Liu, H., Yu, X., Li, K., Klejnot, J., Yang, H., Lisiero, D., and Lin, C. (2008). Photoexcited CRY2 interacts with CIB1 to regulate transcription and floral initiation in *Arabidopsis*. Science 322, 1535–1539.
Mayans, O., van der Ven, P.F.M., Wilm, M., Mues, A., Young, P., Fürst, D.O., Wilmanns, M., and Gautel, M. (1998). Structural basis for activation of the titin kinase domain during myofibrillogenesis. Nature 395, 863–869.
Meyer, K.D., Saletore, Y., Zumbo, P., Elemento, O., Mason, C.E., and Jaffrey, S.R. (2012). Comprehensive analysis of mRNA methylation reveals enrichment in 3′ UTRs and near stop codons. Cell 149, 1635–1646.
Miller, S.M., Wang, T., and Liu, D.R. (2020a). Phage-assisted continuous and non-continuous evolution. Nat Protoc 15, 4101–4127.
Miller, S.M., Wang, T., Randolph, P.B., Arbab, M., Shen, M.W., Huang, T.P., Matuszek, Z., Newby, G.A., Rees, H.A., and Liu, D.R. (2020b). Continuous evolution of SpCas9 variants compatible with non-G PAMs. Nat Biotechnol 38, 471–481.
Min, H.Y., and Lee, H.Y. (2022). Molecular targeted therapy for anticancer treatment. Exp Mol Med 54, 1670–1694.
Morrison, M.S., Podracky, C.J., and Liu, D.R. (2020). The developing toolkit of continuous directed evolution. Nat Chem Biol 16, 610–619.
Mosquna, A., Peterson, F.C., Park, S.Y., Lozano-Juste, J., Volkman, B.F., and Cutler, S. R. (2011). Potent and selective activation of abscisic acid receptors *in vivo* by mutational stabilization of their agonist-bound conformation. Proc Natl Acad Sci USA 108, 20838–20843.
Nemoto, K., Kagawa, M., Nozawa, A., Hasegawa, Y., Hayashi, M., Imai, K., Tomii, K., and Sawasaki, T. (2018). Identification of new abscisic acid receptor agonists using a wheat cell-free based drug screening system. Sci Rep 8, 4268.
Nishimura, N., Sarkeshik, A., Nito, K., Park, S.Y., Wang, A., Carvalho, P.C., Lee, S., Caddell, D.F., Cutler, S.R., Chory, J., et al. (2010). PYR/PYL/RCAR family members are major *in-vivo* ABI1 protein phosphatase 2C-interacting proteins in *Arabidopsis*. Plant J 61, 290–299.
Packer, M.S., Rees, H.A., and Liu, D.R. (2017). Phage-assisted continuous evolution of proteases with altered substrate specificity. Nat Commun 8, 956.
Park, S.Y., Qiu, J., Wei, S., Peterson, F.C., Beltrán, J., Medina-Cucurella, A.V., Vaidya, A.S., Xing, Z., Volkman, B.F., Nusinow, D.A., et al. (2023). An orthogonalized PYR1-based CID module with reprogrammable ligand-binding specificity. Nat Chem Biol 20, 103–110.
Qi, L.S., Larson, M.H., Gilbert, L.A., Doudna, J.A., Weissman, J.S., Arkin, A.P., and Lim, W.A. (2013). Repurposing CRISPR as an RNA-guided platform for sequence-specific control of gene expression. Cell 152, 1173–1183.
Rakonjac, J., and Model, P. (1998). Roles of pIII in filamentous phage assembly. J Mol Biol 282, 25–41.
Richter, M.F., Zhao, K.T., Eton, E., Lapinaite, A., Newby, G.A., Thuronyi, B.W., Wilson, C., Koblan, L.W., Zeng, J., Bauer, D.E., et al. (2020). Phage-assisted evolution of an adenine base editor with improved Cas domain compatibility and activity. Nat Biotechnol 38, 883–891.
Riechmann, L., and Holliger, P. (1997). The C-terminal domain of TolA is the coreceptor for filamentous phage infection of *E. coli*. Cell 90, 351–360.
Rodriguez, P.L., Lozano-Juste, J., and Albert, A. (2019). PYR/PYL/RCAR ABA receptors. In: Seo M, Marion-Poll A, eds. Advances in Botanical Research. New York: Academic Press 51–82.
Roundtree, I.A., Luo, G.Z., Zhang, Z., Wang, X., Zhou, T., Cui, Y., Sha, J., Huang, X., Guerrero, L., Xie, P., et al. (2017). YTHDC1 mediates nuclear export of N^6-methyladenosine methylated mRNAs. eLife 6, e31311.
Shi, H., Xu, Y., Tian, N., Yang, M., and Liang, F.S. (2022). Inducible and reversible RNA N^6-methyladenosine editing. Nat Commun 13, 1958.
Stanton, B.Z., Chory, E.J., and Crabtree, G.R. (2018). Chemically induced proximity in biology and medicine. Science 359, eaao5902.
Stratton, M.R. (2011). Exploring the genomes of cancer cells: progress and promise. Science 331, 1553–1558.
Stratton, M.R., Campbell, P.J., and Futreal, P.A. (2009). The cancer genome. Nature 458, 719–724.
Sun, X., Zhou, C., Xia, S., and Chen, X. (2023). Small molecule-nanobody conjugate induced proximity controls intracellular processes and modulates endogenous unligandable targets. Nat Commun 14, 1635.
Thuronyi, B.W., Koblan, L.W., Levy, J.M., Yeh, W.H., Zheng, C., Newby, G.A., Wilson, C., Bhaumik, M., Shubina-Oleinik, O., Holt, J.R., et al. (2019). Continuous evolution of base editors with expanded target compatibility and improved activity. Nat Biotechnol 37, 1070–1079.
Li, J., Chen, Z., Chen, F., Xie, G., Ling, Y., Peng, Y., Lin, Y., Luo, N., Chiang, C.M., and Wang, H. (2020). Targeted mRNA demethylation using an engineered dCas13b-ALKBH5 fusion protein. Nucleic Acids Res 48, 5684–5694.
Wang, X., Lu, Z., Gomez, A., Hon, G.C., Yue, Y., Han, D., Fu, Y., Parisien, M., Dai, Q., Jia, G., et al. (2014). N^6-methyladenosine-dependent regulation of messenger RNA stability. Nature 505, 117–120.
Wang, X., Zhao, B.S., Roundtree, I.A., Lu, Z., Han, D., Ma, H., Weng, X., Chen, K., Shi, H., and He, C. (2015). N^6-methyladenosine modulates messenger RNA translation efficiency. Cell 161, 1388–1399.

Wei, J., Yu, X., Yang, L., Liu, X., Gao, B., Huang, B., Dou, X., Liu, J., Zou, Z., Cui, X.L., et al. (2022). FTO mediates LINE1 m^6 A demethylation and chromatin regulation in mESCs and mouse development. Science 376, 968–973.
Wilson, C., Chen, P.J., Miao, Z., and Liu, D.R. (2020). Programmable m^6A modification of cellular RNAs with a Cas13-directed methyltransferase. Nat Biotechnol 38, 1431–1440.
Xie, V.C., Styles, M.J., and Dickinson, B.C. (2022). Methods for the directed evolution of biomolecular interactions. Trends Biochem Sci 47, 403–416.
Yang, L., Mo, W., Yu, X., Yao, N., Zhou, Z., Fan, X., Zhang, L., Piao, M., Li, S., Yang, D., et al. (2018). Reconstituting *Arabidopsis* CRY2 signaling pathway in mammalian cells reveals regulation of transcription by direct binding of CRY2 to DNA. Cell Rep 24, 585–593.e4.
Ye, X., Tu, M., Piao, M., Yang, L., Zhou, Z., Li, Z., Lin, M., Yang, Z., and Zuo, Z. (2020). Using phage-assisted continuous evolution (PACE) to evolve human PD1. Exp Cell Res 396, 112244.
Yu, J., Shin, J., Yu, J., Kim, J., Yu, D., and Heo, W.D. (2024). Programmable RNA base editing with photoactivatable CRISPR-Cas13. Nat Commun 15, 673.
Zetsche, B., Volz, S.E., and Zhang, F. (2015). A split-Cas9 architecture for inducible genome editing and transcription modulation. Nat Biotechnol 33, 139–142.
Zhao, X., Yang, Y., Sun, B.F., Shi, Y., Yang, X., Xiao, W., Hao, Y.J., Ping, X.L., Chen, Y.S., Wang, W.J., et al. (2014). FTO-dependent demethylation of N^6-methyladenosine regulates mRNA splicing and is required for adipogenesis. Cell Res 24, 1403–1419.
Ziegler, M.J., Yserentant, K., Dunsing, V., Middel, V., Gralak, A.J., Pakari, K., Bargstedt, J., Kern, C., Petrich, A., Chiantia, S., et al. (2021). Mandipropamid as a chemical inducer of proximity for *in vivo* applications. Nat Chem Biol 18, 64–69.

https://doi.org/10.1007/s11427-024-2707-9